Mixed Tunnelling Avalanche Transit Time Mode Analysis of Flat Doping Profile Silicon Carbide Double Drift Region Diodes for Operation in W, D, Y and Thz Bands

Pranati Panda and Gananath Dash*
Electron Devices Group at the School of Physics,
Sambalpur University, Jyoti Vihar, Burla,
Sambalpur – 768019, Odisha, India

***Abstract*—Computer simulation experiment is carried out to explore the prospects of SiC for application as Mixed Tunnelling Avalanche Transit Time diode in a wide ranging frequency from 0.1 THz to 1.0 THz. We have obtained a commendable power output of 2.85 W at 0.81 THz with an efficiency of 16%. The not so high noise measure of 25.6 dB at the same frequency is a clear manifestation of the 24.87% tunnelling current which ascertains the advantage of SiC in mixed mode operation.**

***Keywords*—4H-SiC, IMPATT, MITATT, Tunnelling**

I. INTRODUCTION

Silicon Carbide (SiC) has some exotic properties which make it the most suitable for modern power electronics. It is recognized as an excellent wide band gap (WBG) semiconductor for high temperature and high speed devices [1-5]. There are many different poly-types of SiC such as 3C, 2H, 4H, 6H, 9H etc. Out of them only 4H-SiC and 6H-SiC are commercially available. 4H-SiC is the most widely explored material [6-8] for high power devices because its carrier mobility is better than that of 6H-SiC. Many reports establish the superiority of 4H-SiC over 6H-SiC [9-11]. Yuan *et al.* [12, 13] and Zhao *et al.* [14] have reported some experimental as well as theoretical results for the first time with a 4H-SiC IMPATT oscillator operating at X and Ka band of frequencies. They have considered the DC and high power generation aspects of the IMPATT diode. They have reported that the diode exhibits high efficiency and high power as expected compared to Si and GaAs IMPATT (Impact Avalanche Transit Time) diodes. Pattanaik *et al.* [15] have reported the performance of 6H-SiC based DDR (Double Drift Region) IMPATT diodes with reference to DC and microwave properties as well as noise characteristics. They have compared the results with those of Si and GaAs based IMPATT diodes under similar operating conditions at the D band. All these reports however do not consider the effect of tunnelling current on the diode properties. When the diode operation is envisaged at THz frequencies the diode active region becomes so thin that it is almost impossible to avoid tunnelling of carriers. The diode operation in such situation is referred to as MITATT (Mixed Tunnelling Avalanche Transit Time) mode. Therefore, the authors in this paper have analyzed in detail the DC, small signal and noise characteristics of 4H-SiC MITATT diodes for operation in W, D, Y and THz band of frequencies. A power output of 2.85 W at 0.81 THz with an efficiency of 16%, obtained from our simulation results for the SiC MITATT diode, is noteworthy. In addition the fact that the noise measure at the same frequency is not so high (25.6 dB) may be reckoned as an additional advantage of SiC particularly for MITATT mode operation.

II. THEORY

A. General

A generalised method of analysis for DC and small-signal characterisation of a MITATT diode has been presented by Dash and Pati [16]. Similarly Dash *et al.* have presented a MITATT mode noise simulation scheme [17] which can be used for any diode structure made from any semiconductor. We have extended them to incorporate parabolic barriers and briefly describe them in the following subsections. The reader can however, refer to the original publications for more detail.

B. DC Analysis

A schematic of the n^+npp^+ diode structure under consideration, along with the band picture, is shown in Fig. 1. We considered a purely field dependent tunnelling generation rate of the form

$$g_{Tn}(x) = A_T E^2(x) \exp\left[\frac{-B_T}{E(x)}\right], \quad (1)$$

where the co-efficients A_T and B_T, for a parabolic barrier, can be expressed as

$$A_T = \frac{q^2}{4\pi^3\hbar^2}\left(\frac{2m^*}{E_g}\right)^{\frac{1}{2}}, \quad (2)$$

and

$$B_T = \frac{\pi}{2q\hbar}\left(\frac{m^* E_g^3}{2}\right)^{1/2}. \quad (3)$$

The tunnelling generation rate for holes is obtained by considering the energy band diagram of a reverse biased p-n junction as shown in Fig. 1. The tunnel generation of an electron at x' is simultaneously associated with the generation of a hole at x, where $(x - x')$ is the spatial separation between the edges of the conduction band and the valence band at the same energy level and is a function of x. Therefore, the tunnel generation rate for holes can be linked to that for electrons as $g_{Tp}(x) = g_{Tn}(x')$.

(This work is licensed under a Creative Commons Attribution 4.0 International License.)

The position x' can be derived from the position x in the following way. The electrical potential in the depletion layer of a diode can be determined as a function of x by integrating Poisson's equation twice (neglecting the presence of mobile space charge) from which the energy of the electron as a function of x can be determined. Taking U as a measure of energy from the lowest level of the conduction band on the n-side of the diode and making use of the idea that the vertical difference between x and x' is the band gap E_g, x' can be easily obtained in terms of x by referring to Fig. 1 as [16]

$$x' = x\left[1 - \frac{E_g}{U}\right]^{1/2} \quad \text{for} \quad 0 \leq x \leq x_j \tag{4}$$

and

$$x' = W - (W - x)\left[1 - \frac{E_g}{U_B - U}\right]^{\frac{1}{2}} \quad \text{for} \quad x_j \leq x \leq W \tag{5}$$

where x_j is the junction point and is measured from the surface. The electrons in the valence band between $x = 0$ and $x = x_1$ (Fig. 1) would have no available states in the conduction band for tunnelling. Consequently the hole generation rate due to tunnelling within this region is zero. Similarly, non-availability of electrons to tunnel to the energy states in the conduction band between $x = x_2$ and $x = W$ (Fig. 1) results in no tunnelling of electrons in this region. These phenomena are incorporated into our simulation scheme.

Using $J = J_p + J_n$ = constant and making a change of variable, $P(x) = \{J_p(x) - J_n(x)\}/J$, the steady-state combined carrier continuity equation can be recast into the form

$$\frac{\partial P(x)}{\partial x} = (\alpha_p + \alpha_n) + (\alpha_p - \alpha_n)P(x) + \frac{q}{J}\{g_T(x) + g_T(x')\}. \tag{6}$$

The Poisson's equation including mobile space charge at any point x in the depletion layer of the diode is given by

$$\frac{\partial E(x)}{\partial x} = \frac{q}{\varepsilon}\{N_D(x) - N_A(x) + p(x) - n(x)\}. \tag{7}$$

The net mobile space charge concentration $(p - n)$ at any space point can be obtained from as

$$q\frac{\partial(p-n)}{\partial x} = J\left(\frac{\alpha_n(x)}{v_p} + \frac{\alpha_p(x)}{v_n}\right) - q\{\alpha_n(x) - \alpha_p(x)\}(p - n) + q\left(\frac{g_T(x)}{v_n} + \frac{g_T(x')}{v_p}\right) + \frac{\partial E}{\partial x}K \tag{8}$$

where K is a correction factor [16]. Equations (6), (7) and (8) are now solved simultaneously to obtain the electric field and carrier current profiles subjected to the necessary boundary conditions. The solution starts from the position of field maximum near the metallurgical junction. A double iterative computer method, which performs iterations over the value and location of field maximum, is used. The edges of the

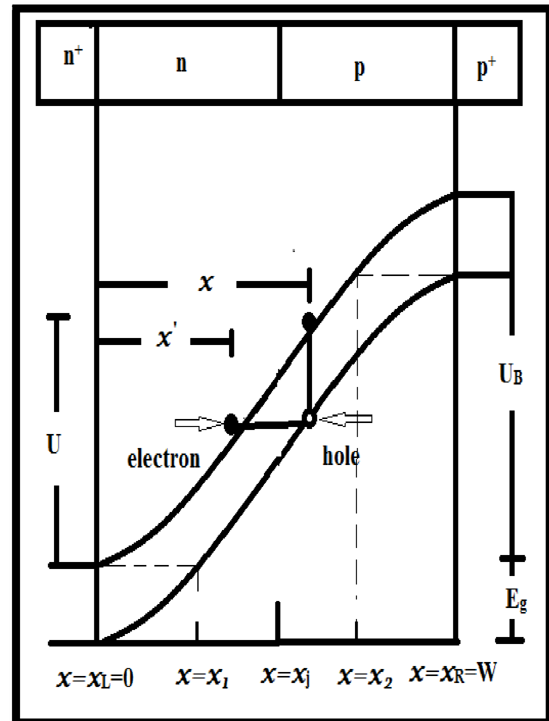

Fig. 1 Schematic and Energy band diagram of a MITATT diode

generation region x_g, can be determined from the conditions $|P(x)| = 0.95$. The drift zone is determined as $(W - x_g)$. The voltage drops across the different zones are determined by integrating the electric field over the respective zones. The diode breakdown voltage (V_B) is the sum of generation region voltage drop (V_g) and drift zone voltage drop (V_D).

C. Small-Signal Analysis

A small-signal method of analysis including the tunnelling current to the conduction as well as displacement current is presented in this subsection. An iterative and generalized computer method is developed to study the small-signal behaviour and this method has the advantages of its applicability to any diode structures. The DC results obtained for any structure under particular operating conditions through the method described in the previous subsection are used as input for the small-signal analysis. We briefly describe the small-signal simulation method below.

The small-signal simulation basically solves two simultaneous differential equations (9) and (10) using a modified Runge-Kutta approach subject to the required boundary conditions. Since the initial values of R and X are not known, iterations are performed over those until the boundary conditions are met.

$$D^2R + (\alpha_n - \alpha_p)DR - 2r_n\frac{\omega}{\bar{v}}DX + \left[\frac{\omega^2}{\bar{v}^2} - H - \frac{qr_p}{\bar{v}\,\varepsilon}\left(g'_T(x) + g'_T(x')\right)\right]R - \frac{2\bar{\alpha}\omega}{\bar{v}}X = \frac{2\bar{\alpha}}{\bar{v}\varepsilon} \tag{9}$$

(This work is licensed under a Creative Commons Attribution 4.0 International License.)

and

$$D^2X + (\alpha_n - \alpha_p)\,DX + 2r_n\frac{\omega}{\bar{v}}\,DR + \left[\frac{\omega^2}{\bar{v}^2} - H - \frac{2r_p}{\bar{v}\,\varepsilon}\left(g'_T(x) + g'_T(x')\right)\right]X + \frac{2\bar{\alpha}\omega}{\bar{v}}\,R = -\frac{\omega}{\bar{v}^2\varepsilon} \tag{10}$$

where

$$H = (\alpha'_P - \alpha'_n)\,DE_m + \frac{2\bar{\alpha}'J}{\bar{v}\varepsilon}.$$

Once the iteration converges the individual space step contribution of the small-signal resistance $R(x)$ and reactance $X(x)$ are obtained from the solution. The integrated values of the device negative resistance $Z_R = \int_0^W R(x)\,dx$ and device reactance $Z_X = \int_0^W X(x)\,dx$ are then determined. The device conductance (G), and the device susceptance (B) are calculated using the relations

$$G = \frac{Z_R}{Z_R^2 + Z_X^2} \tag{11}$$

$$B = -\frac{Z_X}{Z_R^2 + Z_X^2} \tag{12}$$

The small-signal analysis is repeated for several frequencies and the optimum frequency (f_p) corresponding to diode peak negative conductance $(-G_p)$ is determined. The diode negative resistance $-Z_{R_p}$ at f_p as well as total reactance $-Z_{X_p}$ at f_p can also be computed using this simulation method.

D. Noise Analysis

In avalanche transit time diodes noise in generated due to the random nature of impact ionisation process; therefore we assume the tunnelling to be a quiet process. Further, we assume that the avalanche process consists of a noiseless generation rate g and noise generation rate γ. A noise generating source $\gamma(x')$ located at x' in the depletion region is associated with an element of generated current dJ_C occurring in the interval dx' at x' according to the relation

$$dJ_C = q\gamma(x')dx'. \tag{13}$$

An element of mean square noise current $< di_C^2 >$, in a frequency interval df contributed by dJ_C is obtained from the theory of short noise as

$$< di_C^2 > = 2q\ df\ dJ_C\,A = 2q^2\ df\ \gamma(x')\ A\,dx'. \tag{14}$$

Now, a noise source $\gamma(x')$ located at x' in the generation region gives rise to a noise electric field $e(x,x')$ in the entire depletion layer analogous to the vibration produced along the entire length of a bar when struck at one point. The terminal voltage $v_t(x')$ produced by $\gamma(x')$ is obtained by integrating $e(x,x')$ over x for the whole depletion layer

$$v_t(x') = \int_0^W e(x,x')\,dx\,. \tag{15}$$

A transfer impedance can then be defined as

$$Z_t(x') = \frac{v_t(x')}{I_{cav}(x')}, \tag{16}$$

where $I_{cav}(x') = A\,dJ_C$ is the average current generated in the interval dx' and A is the area of the diode. The mean square noise voltage is now obtained as

$$< v^2 > = 2q^2 df\,A \int |Z_t(x')|^2\ \gamma(x')dx', \tag{17}$$

from which the "Noise Measure" (NM) can be defined as an indicator of noise to power trade off ratio and can be written as

$$NM = \frac{< v^2 >/df}{4kT\,(-Z_R - R_P)}, \tag{18}$$

where k is Boltzman constant, T is absolute temperature, Z_R is the integrated device negative resistance and R_P is the parasitic series resistance.

We have considered four SiC DDR MITATT diodes in this work. The widths of the diodes have been determined to operate in W, D, Y and THz bands, respectively around the centre frequencies of 94 GHz, 140 GHz, 220 GHz and 0.8 THz, in accordance with the guidelines presented in [18]. The doping concentrations are optimized for a punch through electric field profile. The current densities are set for a high efficiency. The area of the diode is calculated following [19]. The optimized structural parameters of the DDR MITATT diodes operating in different frequency bands are presented in Table I.

III. Results and Discussion

The results obtained from the simulation study are discussed in this section under two headings. The DC and small signal properties are analyzed in sub-section III (A). The noise characteristics are presented in sub-section III (B).

A. DC and Small-Signal Behaviours

Some of the important parameters to study the potentials of a MITATT diode are maximum electric field, breakdown voltage, efficiency and the percentage of tunnelling current. The values of these parameters obtained at different frequency bands of operation are listed in Table II. As the frequency band of operation is increased the width of depletion layer is thinned down. As a result the maximum electric field is pushed up. Increase in maximum electric field near the junction results in increase in the number of electrons tunnelling through the junction. So, the percentage of tunnelling current increases. To be more specific we note that as we move from W band to THz band the percentage of tunneling current increases from 10.6% to 24.87%. On the other hand the breakdown voltage decreases from 613 V to 90.8 V when we change the operating band from W to THz. The rapid fall in breakdown voltage as we go from

TABLE I. DESIGN PARAMETERS OF SiC DDR MITATT DIODES FOR OPERATION IN W, D, Y AND THz BANDS.

Band	Width (µm)		Doping (10^{23} m^{-3})		Area (10^{-12} m^2)	J (10^8A/ m^2)
	n-side	*p-side*	*n-side*	*p-side*		
W band	1.230	1.230	1.7	1.7	452.0	3.1
D band	0.787	0.787	2.4	2.4	236.0	5.0
Y band	0.528	0.528	4.0	4.0	87.60	8.0
THz band	0.148	0.148	19.4	19.4	03.58	27

(This work is licensed under a Creative Commons Attribution 4.0 International License.)

TABLE II. DC AND SMALL SIGNAL PROPERTIES OF SIC DDR MITATT DIODES FOR OPERATION IN W, D, Y AND THZ BANDS.

Frequency band	E_{max} (10^8V/m)	V_B (V)	η (%)	f_p (GHz)	G_p(10^{-4} S)	P_{RF} (W)	J_T/J_0 (%)	Z_R (Ω)
W band	3.85	613	18.8	100	-13.3	62.5	10.60	-15.13
D band	4.05	388	17.9	160	-12.6	23.7	11.49	-14.54
Y band	4.34	273	17.6	230	-9.64	8.98	14.29	-13.92
THz band	5.79	90.8	16.0	810	-2.77	2.85	24.87	-13.79

low to high frequency band is due to decrease in widths of the diodes. The efficiency of the diodes under consideration records a minor variation from W band to THz band. This fact is thus indicative of appreciable efficiency (16 %) for the SiC diode even at THz frequencies.

The performance of a power source device is assessed through the study of small-signal properties like negative conductance, negative resistance and power output. The small signal properties of the SiC MITATT diodes for W, D, Y and THz frequency bands are presented in Table II and Fig. 2. It can be seen from Fig. 2 that the peak values of device negative conductance gradually decreases from 1.33×10^{-3} S to 2.77×10^{-4} S as we change the frequency band from W to THz. Moreover, the rapid fall in breakdown voltage as we move from low frequency to high frequency bands reduces the input power to the device with a consequent decrease in output power. As we move from low frequency to high frequency structure the generation region width becomes gradually narrower and the level of tunneling current increases. The device negative resistance shows degradation (Table II) as the level of tunneling current increases from low to high frequency bands. The amount of diode negative resistance is a measure of power output from the device. So, the output power decreases with increase in frequency of operation. From the above discussion we observe that there is a considerable degradation in device properties as we move from W band to THz band. But, this degradation in device properties is accompanied by an improvement in noise behaviour (with increase in frequency band of operation). The details of noise behaviour of the designed SiC MITATT diodes have been discussed in the next subsection.

B. Noise Behaviours

The noise properties of the 4H SiC DDR MITATT diodes considered in this paper are presented in Table III and the variations of mean square noise voltage per bandwidth with respect to frequency for different structures operating in W, D, Y and THz band of frequencies are shown in Fig. 3. As discussed above the percentage of tunnelling current gradually increases from the low frequency to high frequency diodes. Avalanching is a noisy process while tunnelling is a quiet process. So, the height of noise peak steadily decreases with

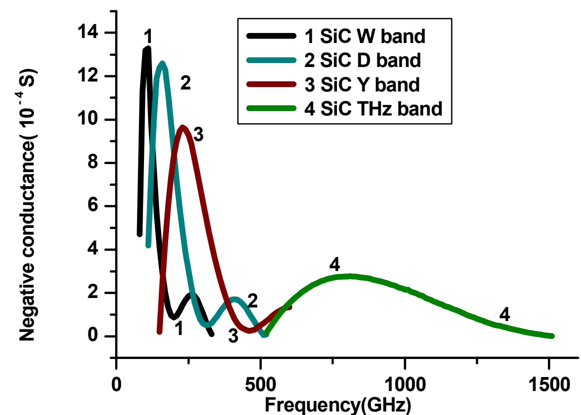

Fig. 2 Device negative conductance as a function of frequency for W, D, Y and THz band SiC flat doping profile DDR MITATT diodes.

increase in percentage of tunnelling current. This behaviour is clearly noticeable from the mean square noise voltage presented in Table III and Fig. 3. It means that higher frequency diodes, which have higher level of tunnelling currents, would be less noisy.

Again, we observe from Fig. 3 that at low frequencies the mean square noise voltage remains almost constant. At medium frequencies it increases rapidly and attains a maximum near the resonant frequency. At higher frequency region it decreases very sharply. Variation of mean square noise voltage per band width versus frequency plot in Fig. 3 agrees with the reports of Hines [20], Gummel and Blue [21] and Haitz and Voltmer [22]. At frequencies above the resonant

TABLE III. NOISE PROPERTIES OF SIC DDR MITATT DIODES FOR OPERATION IN W, D, Y AND THZ BANDS.

Frequency Band	f_g (GHz)	MSNV (10^{-14} V^2s)	f_1 (GHz)	NM (dB)	MSNV at f_p (10^{-16} V^2s)	NM at f_p (dB)
W band	50	1.5	160	26.02	3.26	33.67
D band	60	1.4	220	25.24	2.88	31.45
Y band	90	1.3	350	24.69	2.26	31.38
THz band	280	1.13	1210	21.16	1.04	25.56

MSNV-Mean Square Noise Voltage

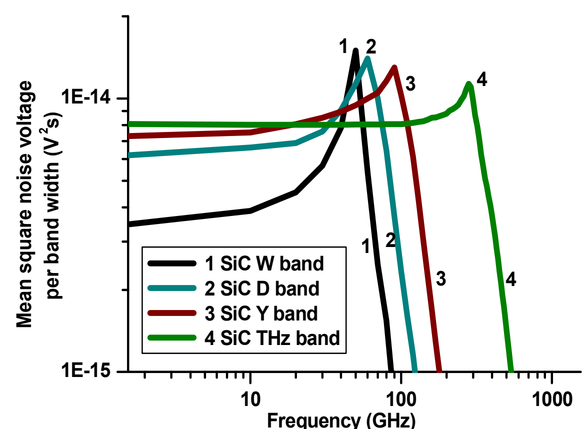

Fig. 3 Mean square noise voltage as a function of frequency for W, D, Y and THz band SiC flat doping profile DDR MITATT diodes.

(This work is licensed under a Creative Commons Attribution 4.0 International License.)

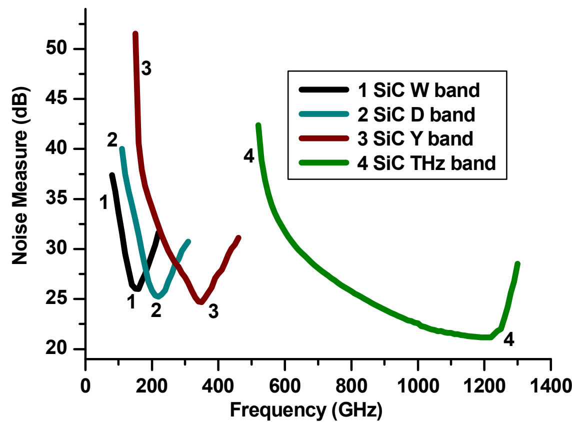

Fig. 4 Noise Measure as a function of frequency for W, D, Y and THz band SiC flat doping profile DDR MITATT diodes.

frequency the negative resistance decreases rapidly and so also the noise voltage. So, the performance of a diode as an amplifier is assessed through the value of noise measure. Noise measure is an indicator of noise to power ratio in MITATT diode. Fig. 4 shows the variation of noise measure with frequency for all the four bands of operation. From the graph we observe that the minimum value of noise measure for a given frequency band occurs at a frequency nearly twice the operating/design frequency. Minimum value of noise measure continuously decreases with increase in tunnelling current as we move from low frequency to high frequency band of operation. This behaviour is similar to that of the mean square noise voltage. It is thus indicative that the noise level in a diode can be controlled by adjusting the tunnelling level.

One of the interesting consequences of tunnelling current is noticeable if we compare our results with those of Pattanaik *et al.* [15]. While Pattanaik *et al.* have obtained a noise measure minimum of 34 dB for a 6H-SiC diode at 140 GHz we have obtained the same of 31.5 dB from a similar diode at the same frequency. The difference of 2.5 dB is clearly attributable to the tunnelling current which makes our diode to operate in MITATT mode whereas the diode of Pattanaik *et al.* was considered in pure IMPATT mode. We thus conclude that mixed mode operation in SiC diodes has a clear advantage of reduction in noise level compared to pure IMPATT mode operation.

IV. CONCLUSION

DC, small-signal and noise properties of 4H-SiC diodes in mixed tunnelling avalanche transit time mode are explored for operation at W, D, Y and THz bands. The trend of results obtained agrees well with those obtained by other authors earlier for other low band gap materials like Si and GaAs [24, 25]. The regular features of the results include decrease in efficiency and power output with increase in the frequency band of operation. The tunnelling current is enhanced with frequency band. This has a twofold effect. First, because of the loss in avalanche phase delay associated with it, the diode negative conductance as well as negative resistance, responsible for useful power from the device, decreases. Second, the noise levels such as the mean square noise voltage and noise measure are suppressed. The state-of-the-art performance of SiC MITATT diode revealed from our simulation at around 1 THz frequency is commendable with a power output of 3 W, at an efficiency of 16%, with a tunnelling current of 25% and at a noise measure level of 22 dB.

REFERENCES

[1] G. Brezeanu, "High performance power diodes on silicon carbide and diamond," The Publishing House of Romania Academy, Vol. 8, pp. 1-14 (2007).

[2] K. Singh, J. A. Cooper, M. R. Meloch, T. P. Chow and J. W. Palmour, "Silicon carbide power schottky and pin diodes," IEEE Transactions on Electron Devices, Vol. 49, pp. 665-672 (2004).

[3] M. C. Traplee, V. P. Madangagly, Q. Zhang, T. S. Surdarsan, "Design rules for field pate edge termination in SiC Schottky diodes," IEEE Transactions on Electron Devices, Vol. 48, pp. 2659-2664 (2001).

[4] D. C. Sheridan, G. Niu, J. N. Merrett, J. D. Cresller, C. Ellis, C. C. Tin, "Design and fabrication of plannar guard ring termination for high voltage silicon carbide diode," Solid State Electronics, Vol. 44, pp. 1367-1372 (2000).

[5] T. A. Baeraky, "Microwave measurements of the dielectric properties of silicon carbide at high temperature," Egypt Journal of Solids, Vol. 25, No. 2, pp. 263-273 (2002).

[6] C. X. Zang, E. X. Zhang, D. M. Fleetwood, R. D. Schrimpf, "Effect of bias on the irradiation and annealing responses of 4H-SiC MOS devices," IEEE Transactions on Nuclear science, Vol. 58, pp. 2925-2929 (2011).

[7] E. A. Imhoff, F. J. Kub, K. D. Hobart, M. G. Ancona, "High performance smoothy tapered junction termination extentions for high voltage 4H-SiC devices," IEEE Transactions on Electron Devices, Vol. 58, pp. 3395-3400 (2011).

[8] H. Zhang, L. M. Tolbert, B. Ozpinee, "Impact of SiC devices on hybrid electric and plug-in hybrid electric vehicles," IEEE Transactions on Industry Applications, Vol. 47, pp. 912-921 (2011).

[9] S. K. Lee, Ph. D. Thesis, "Processing and characterization of SiC (6H and 4H-SiC) contancts for high power and high temperature device application," Kungliga Tekniska Hogskolan, Stockholm, Sweden (2002).

[10] R. K. Parida, A. K. Panda and G. N. Dash, "Comparative study of high frequency characteristics of SiC based SDRs," 16th International Conference on Physics of Semiconductor Devices (2012).

[11] S. R. Pattanaik, J. Pradhan, S. K. Swain, P. Panda and G. N. Dash, "Terahertz characteristics of 6H-SiC and 4H-SiC IMPATT diodes," Proceedings of 16th International Workshop on Physics of Semiconductor Devices, IWPSD, IIT Kanpur, Dec 19-22 (2011) Presented.

[12] L. Yuan, M. R. Melloch, J. A. Cooper and K. J. Webb, "Silicon carbide IMPATT oscillators for high power microwave and millimetre-wave generation," Proceedings IEEE/Cornell Conference on High Performance Devices, pp. 158-167, (2000).

[13] L. Yuan, M. R. Melloch, J. A. Cooper and K. J. Webb, "Experimental demonstration of a silicon carbide IMPATT oscillator," IEEE Electron Devices Lett., Vol. 22(76), pp. 266-268, (2001).

[14] J. H. Zhao, V. Gruzinskis, Y. Luo, M. Weiner, M. Pan, P. Shiktorov and E. Starikov, "Monte-Carlo simulation of 4H-SiC IMPATT diodes," Semicond. Sci. Technol., Vol. 15, No. 11, pp. 1093, (2000).

[15] S. R. Pattanaik, G. N. Dash and J. K. Mishra, "Prospects of 6H-SiC for operation as an IMPATT diode at 140GHz.," Semicond. Sci. Technol., Vol. 20, pp. 299 (2005).

[16] G. N. Dash and S. P. Pati, "A generalised simulation method for MITATT mode operation and studies on the influence of tunnel current on IMPATT properties," Semiconductor Sci. Technology, Vol. 7, pp 222 (1992).

[17] G. N. Dash, J. K. Mishra and A. K. Panda, " Noise in mixed tunnelling avalanche transit time (MITATT) diodes," Solid State Electronics, Vol. 39, No. 10, pp. 1473-1479(1996).

[18] G. N. Dash, "A new design approach for MITATT and TUNNETT mode devices," Solid State Electronics, Vol. 38, No. 7, pp. 1381-1385 (1995).

[19] G. I. Haddad, R. J. Trew, "Microwave solid-state active devices," IEEE Transactions on Microwave Theory and Techniques, Vol. 50, No. 3, pp. 760-779 (2002).

(This work is licensed under a Creative Commons Attribution 4.0 International License.)

[20] M. E. Hines, "Noise theory for the read type avalanche diode," IEEE Trans. On Electron Devices, Vol. ED-13, (1966).

[21] H. K. Gummel and J. L. Blue, "A small signal theory of avalanche noise in IMPATT diodes," IEEE Trans. Electron Devices, Vol. ED-14, p.569 (1967).

[22] R. H. Haitz and F. W. Voltmer, Appl. Physics Letter, Vol. 9, pp. 381 (1966).

(This work is licensed under a Creative Commons Attribution 4.0 International License.)